#### RESEARCH ARTICLE



WILEY

# High-fidelity finite element modeling of the seismic response of prefabricated steel stairs

#### Correspondence

Tara C. Hutchinson, Department of Structural Engineering, UC San Diego. Email: tara@ucsd.edu

#### Funding information

U.S. Forest Service, Grant/Award Number: 19-DG-11046000-16; Graduate Fellowship from the Department of Structural Engineering at UC San Diego

#### **Abstract**

Advancing the seismic resilience of building systems is an active area of research in earthquake engineering. Ensuring safe egress in and out of buildings during extreme events, such as an earthquake, is essential to supporting this effort. To this end, understanding the seismic response of stairs facilitates the robust design of egress systems to ensure they can remain operable after an earthquake. From prior earthquake events and physical experiments, it is understood that stairs with a flight to landing fixed connection at multiple levels within a building are prone to damage. In addition, the stair system with flight to landing fixed attachments may affect the dynamic behavior of the building. To accommodate seismic inter-story drifts, a kinematically free connection between the stairs and landing has been proposed. Herein this connection is referred to as a drift-compatible stair connection. To investigate and aid in the design of such a connection, a unique set of shake table experiments were conducted at the University of Nevada, Reno. In this paper, an overview of these tests is presented, and a high-fidelity finite element model of the tested stair system is used to predict the responses measured during these experiments. Developed in Abaqus, the robustness of the modeled stair unit is investigated considering a variety of contrasting connections, namely, drift-compatible connections, fixed ends and one end fixed and the other free. Results from these numerical simulations offer guidance towards development of simplified models of multi-level stair subsystems. Such models are needed when investigating seismic resilience of building systems across a wider range of hazard levels. Furthermore, best practices observed utilizing the models developed and evaluated herein against experimental data will be useful for subsequent analysis of larger stair tower models, such as the 10story stair system implemented in the NHERI Tall Wood mass timber building with post-tensioned rocking walls, conducted in 2023 at the UC San Diego Large High-Performance Outdoor Shake Table.

This is an open access article under the terms of the Creative Commons Attribution-NonCommercial-NoDerivs License, which permits use and distribution in any medium, provided the original work is properly cited, the use is non-commercial and no modifications or adaptations are made.

© 2024 The Authors. Earthquake Engineering & Structural Dynamics published by John Wiley & Sons Ltd.

<sup>&</sup>lt;sup>1</sup>Department of Structural Engineering, University of California San Diego, San Diego, California, USA

<sup>&</sup>lt;sup>2</sup>Department of Civil and Environmental Engineering, University of Nevada Reno, Reno, Nevada, USA

<sup>&</sup>lt;sup>3</sup>Construction Specialties, Inc., Muncy, Pennsylvania, USA

<sup>&</sup>lt;sup>4</sup>Seismic Isolation Engineering, Inc., Emeryville, Canada



#### KEYWORDS

finite element simulations, nonstructural components and systems, seismic analysis, seismic behavior, stair systems

#### 1 | INTRODUCTION

During extreme events such as earthquakes, safe egress in and out of buildings is essential. From prior earthquake events and physical experiments, it is observed that stair systems are prone to damage. For instance, extensive damage to concrete stairs during the 2008 Wenchuan earthquake was reported by Li and Mosalam. In addition, damage to both concrete and steel stairs in the 2010 Darfield and the 2011 Christchurch earthquakes were significant (e.g., the technical report published by Department of Building and Housing $^2$ ). The latter led to extensive guidance within New Zealand practice to assure more robust performance of stair systems.  $^3$ 

Stairs, spanning from floor to floor, are exposed to multiple-support dynamic excitations caused by relative floor movement during an earthquake. Despite their vulnerability, very limited research has been conducted to understand their complex response during seismic motions. Amongst the most detailed experimental investigations were those conducted by Higgins<sup>4</sup>. Utilizing quasi-static simulated seismic loading, these tests investigated the performance of two full-scale prefabricated steel stair assemblies with landings. Although an interstory drift ratio of 2.5% was attained, large local deformation demands at the stair to landing connections were observed. The overall performance of the stair was observed to strongly depend on the flexibility of these connections. In subsequent research, prefabricated operable steel stairs were incorporated within a 5-story reinforced concrete building tested on the shake table at the University of California, San Diego.<sup>5</sup> Wang et al.<sup>6</sup> summarizes the seismic performance of egress systems in this shake table test program. Despite the integration of capacity-limited designed connections, damage to the stair flight to slab connections, at multiple levels and at drift demands below design targets for the building, was observed. In addition, observed during this shake table test, Wang et al.<sup>7</sup> reported connection plate weld fracture at 0.74% and 1.41% peak interstory drift ratios (PIDRs), and connection plate yielding at 2.75% and 5.46% PIDRs. The severe damage to the stair flight to slab connection at multiple building levels resulted in non-operable stairs. Observations from this full-scale, 5-story stair tower as tested in a building further corroborated the importance of connection deformability on the seismic response of stairs.

To better understand the seismic response of stair systems, computational investigations have been undertaken to complement experimental studies. For example, Sun et al., Tegos et al. and Noorifard and Tabeshpour Studied the effects of stairs on the seismic response of buildings by incorporating the stairs into a numerical model of the building. In the work of Sun et al., the response of a frame-braced structure with and without the stair system is investigated. They found that the existence of the stair system reduces the vibration period of the building and impacts the internal force distribution. Similarly, Tegos et al. found that stair systems stiffen the structure, however, this work revealed the resulting reduction in floor relative displacement due to the presence of stairs. Noorifard and Tabehshpour found that a stair system built with reinforced concrete slab performs as a K-shaped brace in parallel to the stair flight direction and as an inclined shear wall in transverse to the stair run direction. Therefore, stair systems of this type result in stiffening the structural system and reducing the period and lateral displacement of the building. For the first time, Wang and Hutchinson detailed three-dimensional (3D) finite element model (FEM) of the stair subsystem and studied, numerically, the response of steel stairs under uniaxial pseudo-static displacement loading. They performed parametric studies to understand the impact of story height, landing, connection, and geometry of the stairs on the global and local response of this system. These studies provide the impetus for the present study, which focuses on the numerical simulation of the seismic response of stair systems.

From aforementioned prior studies and field observation, it is clear that stairs fixed at multiple levels within a building are prone to damage. To this end, ASCE 7-16, $^{12}$  Section 13.5.10 states that egress stairs and ramps not part of a seismic force-resisting system are required to be detailed to accommodate the seismic relative (floor-to-floor) displacement. This section of the ASCE 7-16 $^{12}$  standard suggests the use of slotted or oversized holes to accommodate the relative displacement without loss of gravity support. To this end, in 2016 and 2018, two shake table programs of full-scale straight-run prefabricated steel stairs with a variety of connection details were conducted at the  $14 \times 14.6$  ft ( $4267 \times 4450$  mm) two degrees of freedom (2-DOF) shake table at the University of Nevada, Reno (UNR). $^{13,14}$  Each phase utilized a similar configuration, that is a straight-run prefabricated steel stair assembly, with the variation focused on the stair connection details.

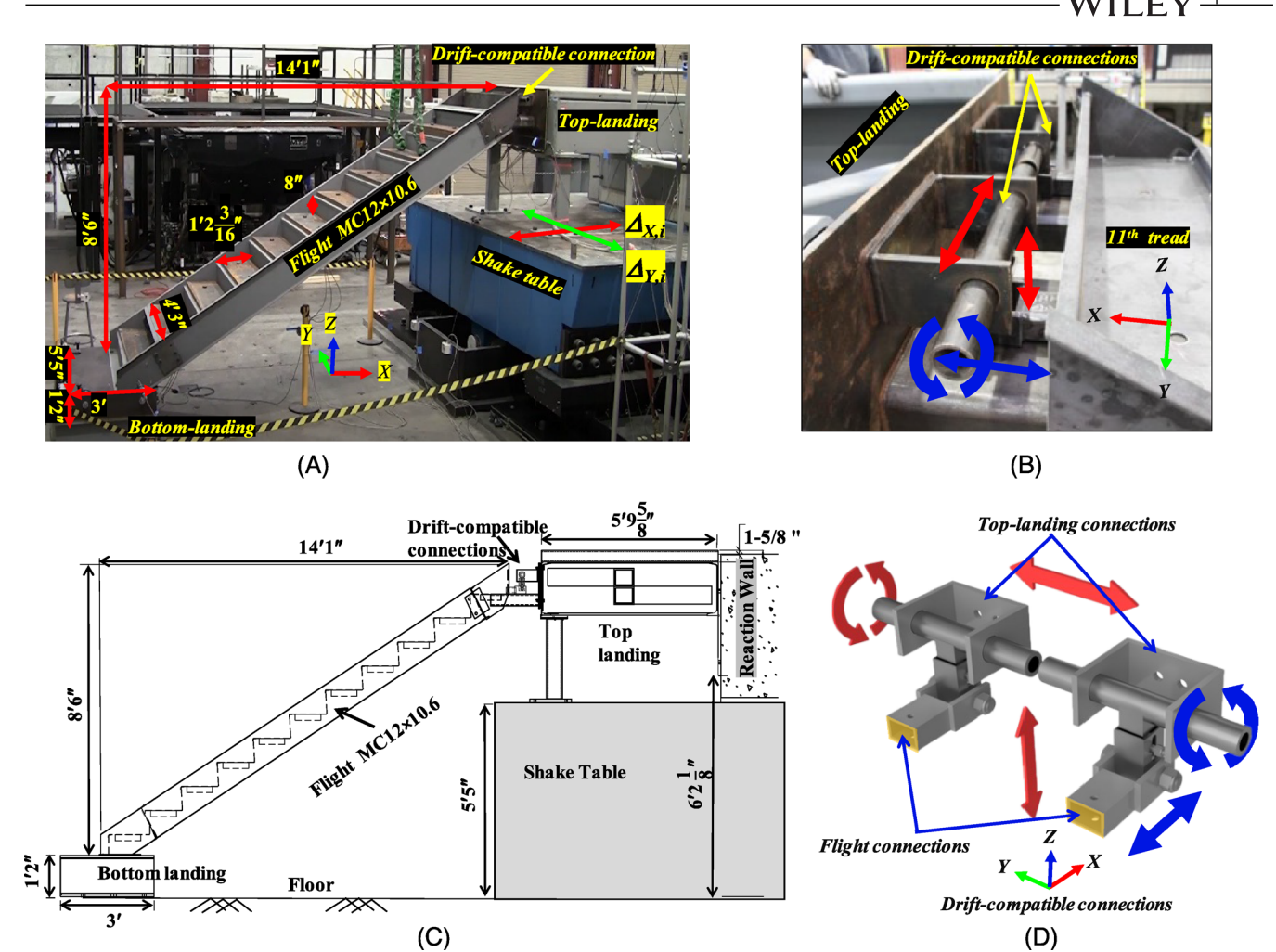


FIGURE 1 (A) Test setup for the fixed-drift-compatible stair specimen, <sup>14</sup> (B) flight to top landing connection, (C) test setup drawing, and (D) drift-compatible (Drift – ready  $^{TM}$ ) connections (1' = 12", 1" = 25.4 mm).

In the first phase, connection details included stairs with a free sliding connection at the bottom (floor) and fixed at the top (landing) (free-fixed) and the stair system fixed at both ends (fixed-fixed). In subsequent tests in 2018 a unique stair with a fixed connection at the bottom and a hanger connection at the top (fixed-drift compatible) were investigated. 13-15 Free-fixed stair systems sustained severe damage during target maximum credible earthquake (MCE) scaled motions. Stairs with drift-compatible connections sustained no damage and performed well under all load levels. To this end, the present paper provides an overview of the shake table test programs at UNR and describes comprehensive FEMs of each of the stair specimens, as developed in Abaqus. 16 Detailed comparisons between the measured test results and predicted numerical response are provided, with a summary of model suggestions offered as a key outcome of the effort herein.

# **EXPERIMENTAL PROGRAM**

## Specimen details and test setup

#### 2.1.1 Flight and landings

The full-scale straight-run stair specimens were each of common geometry and constructed of similar flight and landing arrangements. Notably, the single flight consisted of 11 steps, with a vertical projected height of 8.50 ft (2591 mm), a horizontal projected length of 14.10 ft (4298 mm), and a width of 4.25 ft (1295 mm), see Figure 1A,C. The top landing was connected to the shake table, while the bottom landing was connected to the laboratory reaction floor. The treads and risers were fabricated with 12-gauge plates welded, at both ends, to the stringers. The stringers were continuous

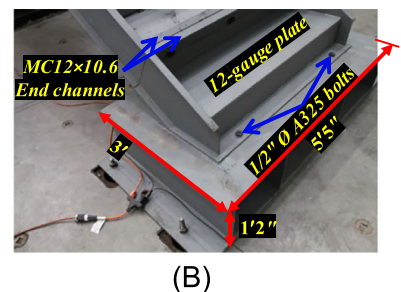


FIGURE 2 Fixed connection details: (A) stair flight to top landing connection, and (B) stair flight to bottom landing connection (1" = 25.4 mm).

members fabricated of MC  $12 \times 10.6$  channels. To incorporate stair systems with different boundary conditions, the stair flights consisted of three main parts. The bottom part consisted of one step and two risers, the middle part consisted of nine steps and nine risers, and the top part consisted of one step and one riser. These parts were connected using MC 12 × 10.6 channels (see Figure 2B). These end channels were each welded to the risers, treads, and stringers. The end channels were connected by six 0.875 in (22.2 mm) diameter ASTM A325 tension control bolts. Specifically, the  $5.25 \times 5.50$ ft (1600  $\times$  1676 mm) top landing consisted of four MC 18  $\times$  42.7 channels at the perimeter. To stiffen the top landing, two  $6 \times 6 \times 0.5$  in  $(152.4 \times 152.4 \times 12.7 \text{ mm})$  Hollow Structural Sections (HSS) were placed diagonally and two  $4 \times 4 \times 0.5$  in  $(101.6 \times 101.6 \times 12.7 \text{ mm})$  HSS were welded at the top of the landing in parallel to the stair flight direction. The top landing was supported, in the vertical direction, on two  $6 \times 4 \times 0.5$  in  $(152.4 \times 101.6 \times 12.7 \text{ mm})$  HSS posts at the corners close to the stair flight. These landing posts were each connected to the landing using three 0.75 in (19.1 mm) diameter ASTM A325 bolts and were connected to the shake table using four 0.875 in (22.2 mm) diameter ASTM A325 bolts. The top landing was installed against a rigid block. The bottom landing consisted of a 1 in (25.4 mm) thick plate supported on four W12 × 16 wide flange beams. The stiffened plate, including the top landing as assembled during the drift-compatible-fixed stair system, is shown in Figure 1. During tests on fixed-fixed and free-fixed stair systems, a gap at the end channel connections was observed due to the flexibility of the end channel. To address this, during the test of a drift-compatible-fixed stair system, stiffener plates were installed at these connections (see Figure 2A).

## 2.1.2 | Stair flight to landing connections

In the free-fixed stair system, the top landing-to-stair flight connection was detailed with a 4 in (101.6 mm) wide 0.25 in (6.35 mm) thick steel plate welded to stringers, which was bolted to the landing. Subsequently, under a target MCE-scaled earthquake, the attachment plate yielded. Hence, to avoid the out-of-plane bending of this plate, two stiffener plates were welded to this connection, see Figure 2A. The movement of the stair on the bottom landing was not constrained along the XY (horizontal) plane, and only supported vertically, thus the stair was freely moving at its bottom landing. In contrast, the fixed-fixed stair system consisted of both the flight-to-top landing connection and the flight-to-bottom landing connection fixed in all degrees of freedom. The connection between the stair flight to the top landing was detailed similar to the free-fixed stair system. As shown in Figure 2B, the stair flight to the bottom landing connection was fixed using four 0.5 in (12.7 mm) diameter ASTM A325 tension control bolts. It should be noted that prior to testing in a fully fixed-driftcompatible connection arrangement, the 2016 tests adopted a top landing stringer connected via a hanger-type connection, thus no vertical support is provided for the stair flight and the straight flight was solely attached, using this hanger type of connection, to the top landing.<sup>13</sup> Transverse movement of the stair flight was naturally observed, even with walking on the stair assembly. Therefore, in the 2018 test program, to refine the design of this general type of connection, driftcompatible connections, with 3-degrees-of-freedom released, were installed at the top landing level along with vertical (gravity) support, see Figure 1B,D. To achieve two-translational and one-rotational displacement release ( $\Delta_Y$ ,  $\Delta_Z$ , and  $\Theta_V$ ), two HSS tube cantilevers extending from the top landing worked as gravity supports and avoided the transverse movements of the stair under service loads. As seen in Figure 1B, the drift-compatible connection has three released (or free) degrees of freedom, the Y, and Z translational degrees of freedom along with the Y rotational degree of freedom. These three degrees of freedom allowed the top landing to move freely, under all load levels, in both transverse and longitudinal directions without imposing large deformations to the stair system, and thus preventing damage to the stair flight and connection. It is also notable that the connection provides a second-dependent release location, as it facilitates a rotational

TABLE 1 Earthquake tests conducted during the 2016 shake table test program (1" = 25.4 mm).

			Max. amplitude in X-direction (inches)		Max. amplitude in Y-direction (inches)	
Test	Test name <sup>a</sup>	Intensity	+	_	+	
1	Test-N	Level 1 <sup>b</sup>	1.1	1.6	1.3	2.4
2	Test-O	Level 2 <sup>c</sup>	1.7	2.5	2.1	3.8
3	Test-O220	Level 2	2.3	3.3	2.8	5.1

<sup>&</sup>lt;sup>a</sup>These test names are per Black et al. <sup>13,14</sup>

TABLE 2 Earthquake tests conducted during the 2018 shake table test program (1" = 25.4 mm).

			Max. amplitude in X-direction (inches)		Max. amplitude in Y-direction (inches)	
Test	Test name	Intensity	+	-	+	_
1	Test-N	Level 1	1.1	2.1	0.9	1.3
2	Test-O	Level 1	0.9	1.3	1.1	2.1
3	Test-P	Level 1	1.4	2.1	1.3	1.2
4	Test-Q	Level 2	1.4	2.0	1.6	3.1

release about the Y-axis and translation release along the X-direction at its connection with the flight, as shown in blue in Figure 1B,D. Note that tests with the drift-compatible top landing connection exclusively incorporate a fixed connection at the bottom landing as shown in Figure 1A.

# 2.2 | Test protocol

In each of the 2016 and 2018 shake table test programs, the stair specimens were subjected to uniaxial and biaxial quasistatic, dynamic, and earthquake motions across a range of amplitudes. Quasi-static cyclic tests were performed under displacement control, at a target rate of 0.25 in/s (6.35 mm/s) in both directions to target amplitudes of 0.5 in (12.7 mm) and 2.5 in (63.5 mm). Subsequently, dynamic tests were performed at a frequency of 0.5 Hz. In addition, a bilinear single degree of freedom (SDOF) building model with a period of 0.35 s was used to generate interstory drift time histories for testing.<sup>13</sup> The SDOF model had a mass of 0.155 kip-s<sup>2</sup>/in (27145 kg), a damping coefficient of 0.279 kip-s/in (48.9 N-s/mm), and a bilinear stiffness definition. The elastic and inelastic stiffnesses of the numerically modeled building were assumed to be 50 kips/in (8756.2 N/mm) and 10 kips/in (1751.2 N/mm), respectively. The yield strength of the model was taken as 28 kips (124550 N), which results in a 0.56 in (14.22 mm) yield displacement. Interstory drift time history responses determined from these analyses were used as table input displacements to investigate the performance of stairs under motions representative of earthquake shaking. In time history analyses of the building model, the Newhall-LA County Fire Station record recorded during the 1994 Northridge earthquake with different scale factors was used. This record has relatively strong shaking in both directions for 8-10 s and results in a strong forward-and-backward displacement pulse. The fixed-fixed stair system was tested under one interstory drift time history. In contrast, three earthquake tests were performed on the stair system with free-fixed connections. The maximum amplitudes in each X (parallel to the stair flight) and Y (transverse to the stair flight) directions are shown in Table 1. The fixed-fixed stair system was tested under only the Y-component of Test-1 in this table. Four earthquake tests were performed on a fixed-drift compatible stair system. These tests are summarized in Table 2.

#### 2.3 | Instrumentation

Displacements and accelerations of the stairs were measured at five locations as shown in Figure 3. Measurements  $D_5$  and  $D_6$  record the displacements of the top of the stair flight, parallel to the stair flight direction, relative to the top landing, whereas measurements  $D_4$  and  $D_1$  record the transverse (Y-direction) absolute displacements at the top and bottom of the

<sup>&</sup>lt;sup>b</sup>Level 1 was intended to target a design basis demand (2.5 % PIDR).

<sup>&</sup>lt;sup>c</sup>Level 2 was intended to target a maximum credible earthquake demand (4.0 % PIDR).

FIGURE 3 Instrumentation plan (1' = 12", 1" = 25.4 mm). <sup>14</sup>

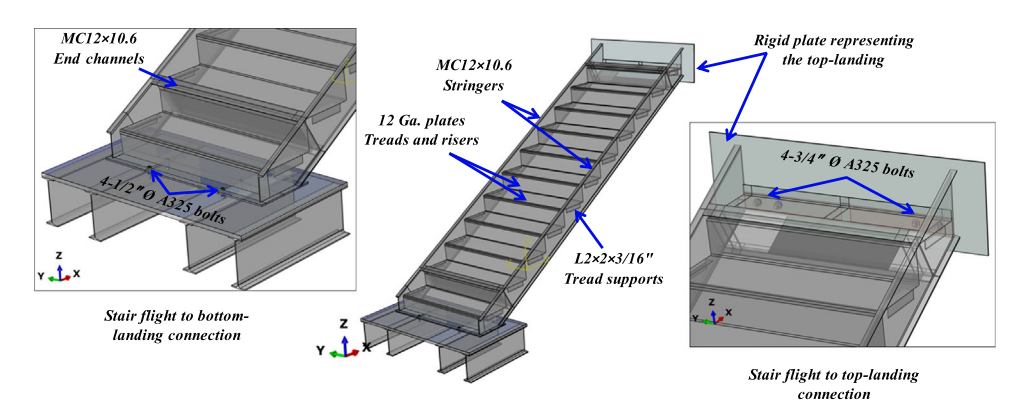


FIGURE 4 Geometry of the fixed-fixed stair system (1" = 25.4 mm).

stair flight, respectively. Measurements  $D_2$  and  $D_3$  are the longitudinal (X-direction) absolute displacements at the bottom of the stair.

# 3 | FINITE ELEMENT MODEL DESCRIPTION

The high fidelity finite element (FE) software Abaqus<sup>16</sup> was used to develop 3D FEMs of the fixed-fixed stair system, free-fixed stair system, and stair system with flight to bottom landing connection fixed and drift-compatible connection installed at the flight to the top landing. Eigenvalue and dynamic analyses were conducted utilizing the various FEMs. The robustness of the FEMs was then evaluated by comparing with the measured responses obtained from the UNR tests. In what follows the details adopted and decisions undertaken in the development of the FEMs are discussed.

# 3.1 | Geometry and simplification

All components of the stair systems were modeled using solid FEs. Since the top landing is rigid and does not have a significant impact on the response of the stairs, it was modeled using only one rigid plate. Figure 4 shows the geometry of the model of the fixed-fixed stair system. In this configuration, both the top and bottom connections are fixed. The geometry of the free-fixed stair system is the same as that of the stair systems with fixed ends, however, there are no bolts at the bottom connection of the free-fixed stair system.

Figure 5 shows the geometry of the model of the stair system with fixed bottom connection and drift-compatible connections installed at the top landing level. In this specimen, to capture the forces at the bottom landing, two load cells in each of the X- and Y-directions were installed along the edge of the bottom landing plate. The bottom landing plate of the stair rested on five HSS tubes, and a layer of grease was applied between the landing plate and the HSS. This resulted in

FIGURE 5 Geometry of the stair system with fixed bottom connection and drift-compatible connections installed at the top landing to stair flight connection (1" = 25.4 mm).

**TABLE 3** Material and finite element types (1 ksi = 6.89 MPa).

Steel section	Expected yield strength (ksi)	Expected ultimate strength (ksi)	Finite element type
A36 Channel	46.8	69.6	C3D8I
A36 plate	46.8	69.6	C3D8I
A36 plate	46.8	69.6	C3D8I
Various	46.8	69.6	C3D8I
ASTM A325	110	132	C3D20
Rigid Material	-	-	C3D8R
A36 plate	46.8	69.6	C3D8R
A500 Gr. B	54.6	69.6	C3D8R
A36 plate	46.8	69.6	C3D8R
	A36 Channel A36 plate A36 plate Various ASTM A325 Rigid Material A36 plate A500 Gr. B	Steel section         strength (ksi)           A36 Channel         46.8           A36 plate         46.8           A36 plate         46.8           Various         46.8           ASTM A325         110           Rigid Material         -           A36 plate         46.8           A500 Gr. B         54.6	Steel section         strength (ksi)         strength (ksi)           A36 Channel         46.8         69.6           A36 plate         46.8         69.6           Various         46.8         69.6           ASTM A325         110         132           Rigid Material         -         -           A36 plate         46.8         69.6           A500 Gr. B         54.6         69.6

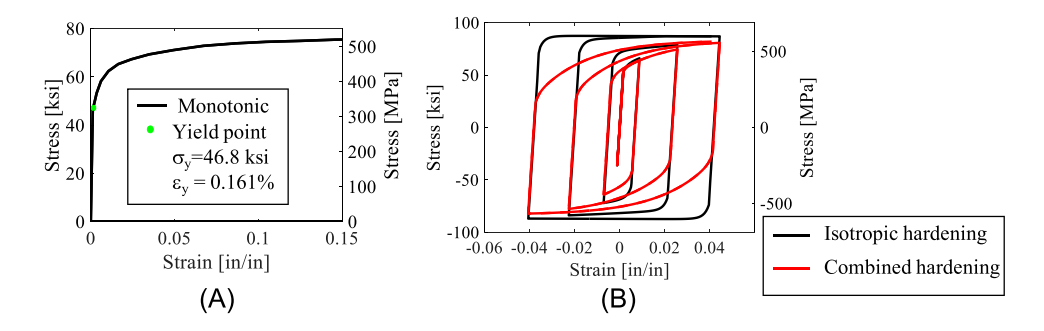


FIGURE 6 Stress-strain curve of A36 steel: (A) Monotonic stress-strain curve (Modified from Wang and Hutchinson<sup>11</sup>), and (B) Cyclic stress-strain curve (Note that combined hardening is synonymous with mixed hardening, i.e., isotropic and kinematic hardening).

small rotations of the bottom landing during the experiment. In numerical simulations, to impose rotation to the bottom landing, four linear elastic springs (two springs in the X-direction, and two springs in the Y-direction), one at each corner, with a stiffness of 5 kips/in (875.63 N/mm) were modeled. Since the springs are linear elastic, using a single iteration, the stiffness of springs was adjusted such that the rotation recorded by string potentiometers  $D_1$ ,  $D_2$ , and  $D_3$  were achieved.

# 3.2 | Material properties

The steel sections and material types used in the tests are summarized in Table 3. Material test data for the stair components were not available in this shake table test. Therefore, in this study, a typical material stress-strain response previously used by Wang and Hutchinson<sup>11</sup> was used to define the stress-strain relation for the half-cycle (Figure 6A) of the material models in Abaqus with expected material properties from prior mill certification of mild ASTM A36 steel. In Abaqus, plastic material models with isotropic and combined cyclic hardening rules were used to model the attachment plates and end channels, the bottom and top parts of the stair flight. Figure 6B shows the cyclic stress-strain response of ASTM



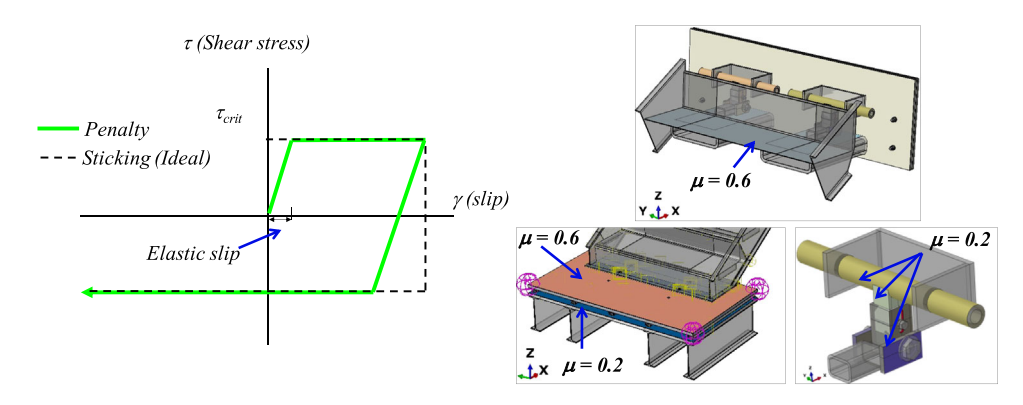


FIGURE 7 (A) Assumed friction model<sup>16</sup> and (B) surfaces with penalty friction model are highlighted.

A36 material determined using a single shell element under uniaxial displacement loading. Since the stair systems in this study do not show large inelastic deformation, both material models showed approximately the same response. However, as shown in Figure 6B, under large plastic strains, the material model with isotropic hardening overestimates the yield strength of the elements. Since no inelastic behavior is expected in the middle region of the stair flight, bottom landing, and bolts, these elements were modeled using an elastic material.

# 3.3 | Boundary conditions

For all FEMs of the various stair systems, the bottom of the I-beams was defined as a fully fixed (encastre) type boundary condition, in which the rotation and translation degrees of freedom in all three directions are zero. In the tests, the top landing of the stair was constructed on the shake table against a rigid block. Except for the translation of the top landing in the X- and Y-directions, all other degrees of freedom were assumed to be zero. In the same manner, in the dynamic analyses, the rigid plate representing the top landing has two free translational degrees of freedom. However, during eigenvalue analyses, all degrees of freedom of the top landing should be constrained.

## 3.4 | Friction model

Interactions between components of the stairs were modeled using surface-to-surface contact elements with a friction model. In the friction model, the penalty formulation shown in Figure 7A is adopted. Figure 7B shows the surfaces with contact elements in various colors. It is noted that the original model (e.g., dashed line in Figure 7) utilized to capture the shear stress and corresponding slip of the surfaces in contact resulted in convergence issues. To this end, the penalty formulation with isotropic directionality, and a small 0.005 unit elastic slip was assumed. In Abaqus, using Equation (1), the critical shear stress ( $\tau_{crit}$ ) is determined based on the contact pressure (p) between two surfaces and the friction coefficient ( $\mu$ ) provided by the user. The contact pressure is determined by the Abaqus solver based on the normal forces developed at each surface in contact, and the surface area. The friction coefficients between components of the stair systems were not measured in the laboratory. Therefore, the friction coefficients used in this study (see Figure 7B) are per the Fastener Design Manual by Barrett. In this design manual, a variety of material friction coefficients are summarized. Notable to the study herein, the static and sliding friction coefficients (kinetic coefficient of friction) between two dry mild steels are 0.74 and 0.57, respectively. The sliding friction coefficient between two mild steel surfaces with grease between them is reported as 0.19. Thus, in the current paper, considering the sliding state, for the dry surfaces of the steel to steel a friction coefficient of 0.6 was assumed, while, for the greased surfaces of steel to steel, a friction coefficient of 0.2 was assigned.

$$\tau_{crit} = \mu \times P \tag{1}$$

# 3.5 | Finite element selection and mesh generation

Various types of FEs were used to model the behavior of the major stair components, as noted in Table 3. To avoid hourglassing and shear-locking effects that are often problematic with the use of solid elements, the C3D8I element, an 8-node

FIGURE 8 Details of the finite element mesh generation.

linear brick element with incompatible modes, was used to model the components of stairs whose bending behavior is critical. In contrast, the C3D8R element, an 8-node linear brick element with reduced integration points, which is computationally more efficient than C3D8I, was used to model components with less likelihood of bending-induced behavior, in this case, ideal for the landings. The landing components were meshed using a coarse mesh with a global seed size of 2. The end regions of the stair flight were meshed using a fine mesh with a global seed size of 0.5, while the middle regions of the flights were meshed using a moderate mesh with a global seed size of 1.5. The drift-compatible connections were modeled with a fine mesh using a global seed size of 0.5. The bolts were meshed using a global seed size of 0.11. Figure 8 shows the generated mesh of the fixed-drift compatible stair system. Note that mesh sensitivity analysis was performed, and the selected mesh sizes are the converged mesh sizes. Refining the mesh size beyond that shown in Figure 8 does not significantly modify the modal characteristics and dynamic responses of stair systems. Additional guidance regarding element selection and mesh generation within commercial software was sought in literature. In the contraction of the stair systems are the converged mesh sizes and dynamic responses of stair systems.

## 3.6 | Analysis procedures

After applying the boundary conditions and defining the contact model, dynamic analysis was performed in three steps. In the first step, the bolts were post-tensioned. In the second step, gravity analysis was conducted. Finally, interstory drift histories were imposed dynamically in the final step. A dynamic implicit solver, namely the Hilber-Hughes-Taylor integrator, with default parameters ( $\alpha = -0.41421$ ,  $\beta = 0.5$ , and  $\gamma = 0.91421$ ) was used as a time integration operator to perform the nonlinear analysis. All dynamic implicit solvers in Abaqus have numerical damping. However, to minimize the numerical damping the maximum time increment should remain small enough (e.g., smaller than 5% of the fundamental period of the model). In the dynamic analysis, Rayleigh damping was used with a critical damping ratio of 2% at the two predominate modes of each stair system. Linear perturbation analysis was performed to determine the modal properties of the stair systems. During linear perturbation analysis, the model's response is defined by its linear elastic stiffness at the base state.

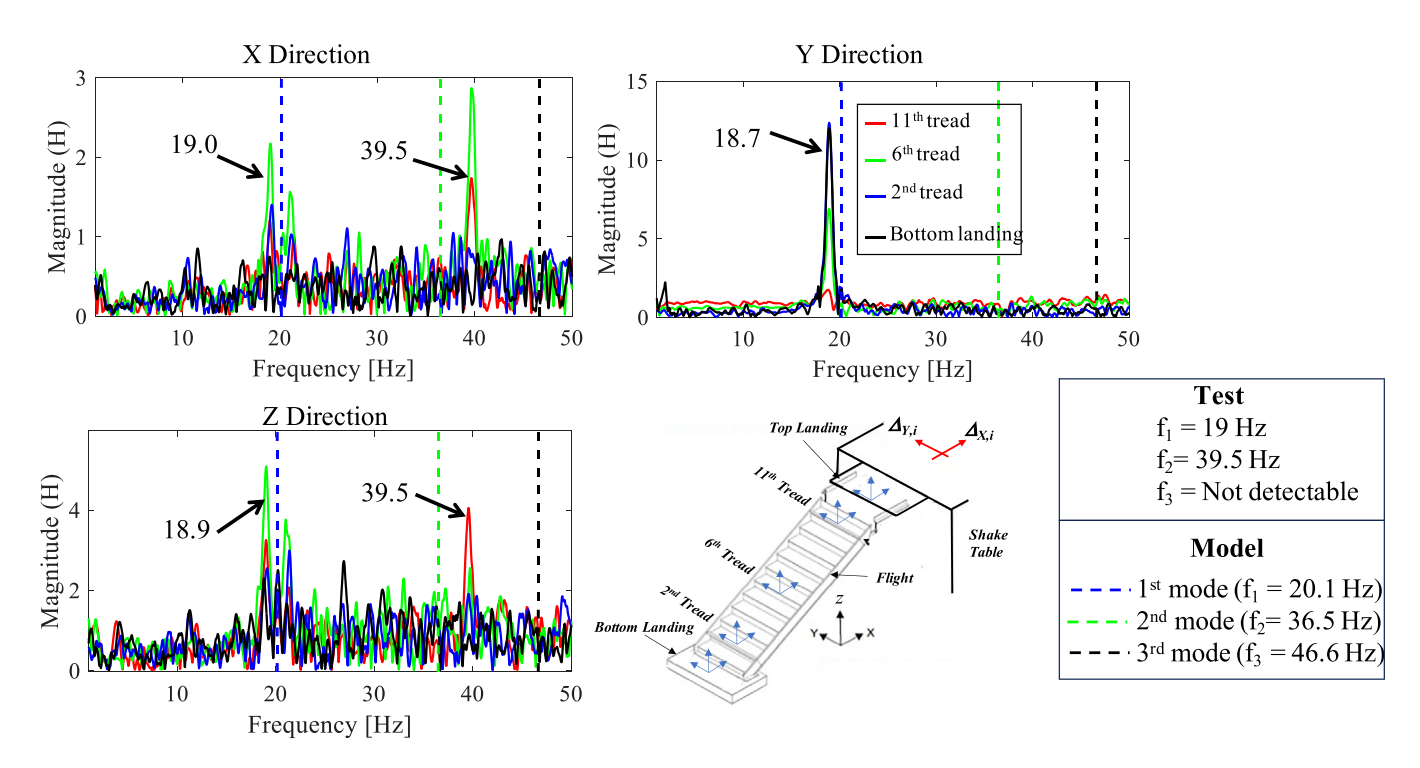
#### 4 | MODEL VALIDATION

The developed FEMs were evaluated through comparisons with the measured responses obtained during the experiments. Initially, to evaluate the robustness of the model, the dynamic characteristics of the stair systems were determined by conducting an eigenvalue analysis. The natural frequencies of stair systems determined by FE analysis were compared to those estimated based on the Frequency Response Function (FRF) developed utilizing measured acceleration responses. For further evaluation of the proposed FEM of the stair systems with various flight-to-landing connections, the displacement time histories and peak acceleration responses from the dynamic analyses were compared to the measured responses from the tests.

(C)

(B)

Mode shapes of fixed-fixed stair system: (A) 1st mode, (B) 2nd mode, and (C) 3rd mode.



FRF computed using measured acceleration responses of the fixed-fixed stair system. FRF, Frequency Response Function.

#### 4.1 Eigenvalue analysis

(A)

#### 4.1.1 Fixed-fixed stair system

The first three natural frequencies from eigenvalue analyses of the stair systems were compared to the estimated natural frequencies from an FRF computed using the measured acceleration responses. The first three mode shapes of the fixedfixed stair system are shown in Figure 9. The first mode, with a natural frequency of 20.1 Hz, of this stair, corresponds to the transitional mode of the stair in the transverse direction. It is noted that although, in the design phase, it was assumed that the bottom landing is fixed, the I-beams are still flexible in their weak axis direction and this contributes to the first mode of the stair system. This mode is also visible in test results (see Figure 10). The second mode, with a natural frequency of 36.5 Hz, of the stair, corresponds to the vibrational mode of the stair flight in perpendicular to the stair run direction (X and Z-directions). The torsional vibration mode of the stair, with a natural frequency of 46.6 Hz, is identified as the third mode of the stair system fixed at both ends.

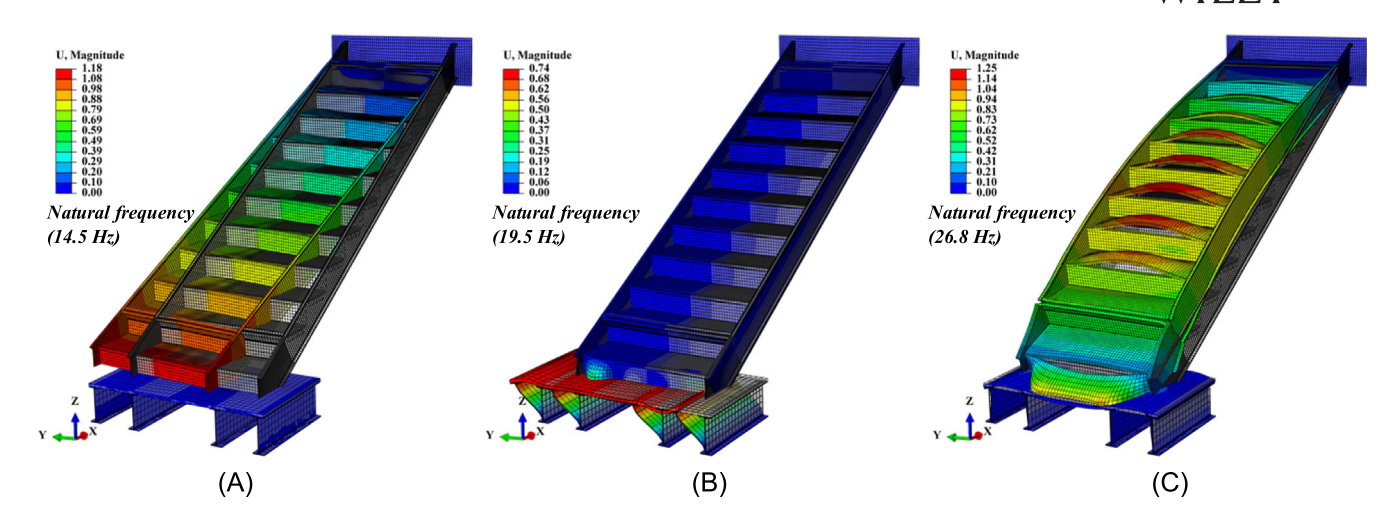


FIGURE 11 Mode shapes of the free-fixed stair system: (A) 1st mode, (B) 2nd mode, and (C) 3rd mode.

The FRF in the experimental eigenvalue analysis is also referred to as the Transfer Function (H) between the input and output signal. This method is also referred to as an input-output System Identification (SI) method. In this study, the input signal is the acceleration recorded at the top landing and the output signal is the acceleration recorded throughout the stair height and the bottom landing. Since, in these test programs, no white noise tests were conducted. In this paper, the actual earthquake test data were used in FRF calculations. In general, the white noise test is conducted with a root mean square amplitude of 3-5%g. Therefore, in this paper, the acceleration data that are smaller than 10%g were used in FRF calculations. The H can then be computed as the ratio between the Cross Spectral Density of the input and the output  $(\sigma_{input.output})$  and the Auto Spectral Density of the input  $(\sigma_{input.input})$ . For the stair systems with fixed-free and fixed drift-compatible boundaries, no windowing is applied to the signals. However, for stair systems with fixed-fixed boundary conditions, to increase the visibility of modes with high vibration frequency a Hamming window with a length of 25% of that of the data and 50% overlap is applied. The resulting magnitude of H is shown in Figure 10. In this work, the Savitzky-Golay Finite Impulse Response (FIR) filter of polynomial order 5 and frame length of 201 is used to smooth the Transfer Function plots. In addition, for comparison purposes, the first three natural frequencies predicted by eigenvalue analysis are also plotted as vertical dashed lines. The dashed lines match the identified peaks of the experimentally computed Transfer Functions reasonably well. In addition, the amplitudes of the Transfer Functions at different sensor locations compare favorably with the mode shapes predicted using FE analysis.

## 4.1.2 | Free-fixed stair system

Similarly, the first three mode shapes of the free-fixed stair system were computed with the FEM and shown in Figure 11. The first mode of this stair assembly is the vibrational mode in the transverse to flight direction with a natural frequency of 14.5 Hz. The vibration of the bottom landing in the Y-direction with a natural frequency of 19.5 Hz contributes to the second mode of the stair assembly, and the third vibration mode with a natural frequency of 26.8 Hz corresponds to the vibration of the stair flight in the perpendicular to the stair run direction, which has components in both X and Z directions.

Similar to the comparative strategy adopted when modeling fixed-fixed stairs, evaluation of the FEM is undertaken to compare with estimated natural frequencies determined via FRFs of the measured accelerations, see Figure 12. Unlike the fixed-fixed stair system, the free-fixed stair systems are more flexible. The analysis results for the first and third modes match well with those of the experiments. However, a larger difference (approximately 15%) between the eigenvalue analysis and experimental results exists for the second mode. The second mode engages the vibration of the bottom landing in the Y-direction. Since the free-fixed stair system is not attached to the bottom landing, the effect of bottom-landing vibration on the stair system response is minimal. Using the C3D8R element, an 8-node linear brick element with reduced integration points may contribute to the nominal 15% difference. Using quadratic element (e.g., C3D20, a 20-node quadratic brick element) or linear element with incompatible modes (e.g., C3D8I, an 8-node linear brick with incompatible modes) would result in improved comparison with the experimental results. However, in this study, since the impact of bottom landing is minimal on the dynamic response of this stair system, and the differences are not significantly large, the computationally more efficient element (C3D8R) is preferred.

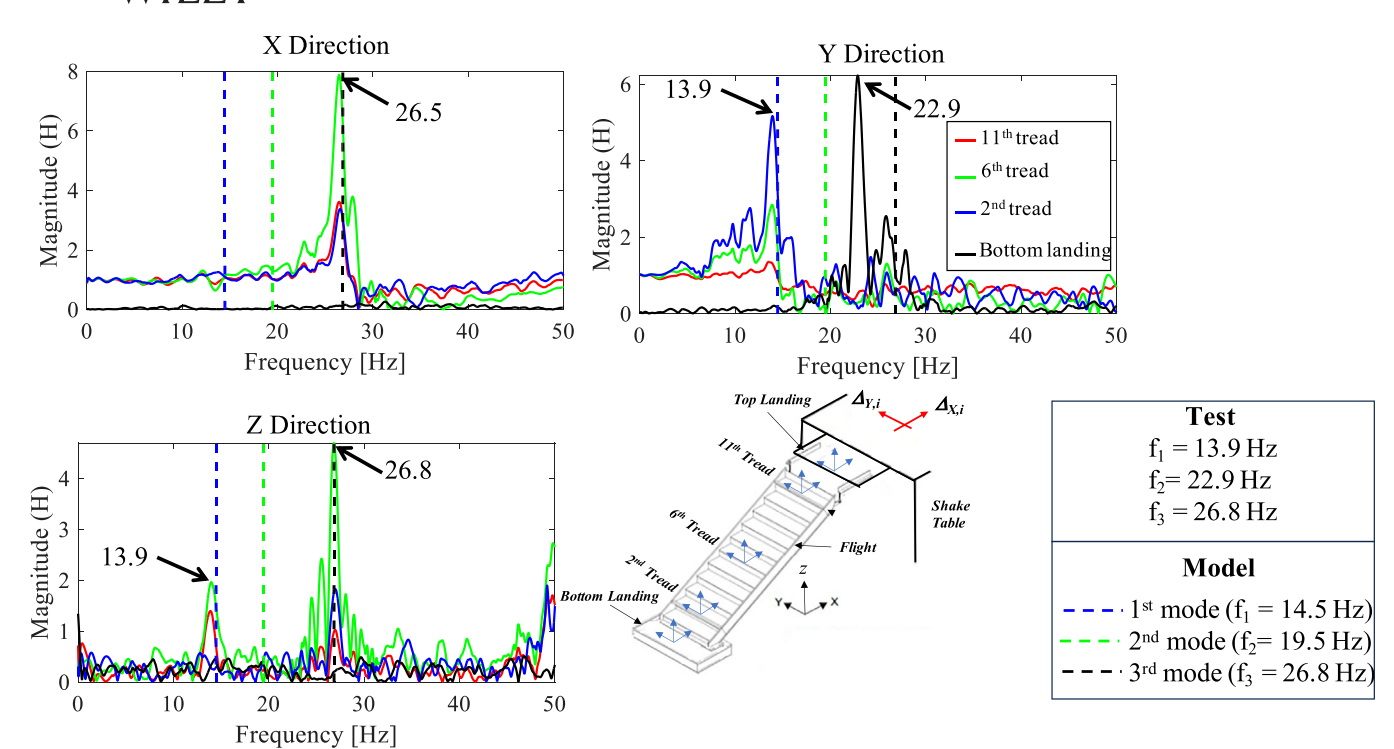


FIGURE 12 FRF computed using measured acceleration responses of free-fixed stair system. FRF, Frequency Response Function.

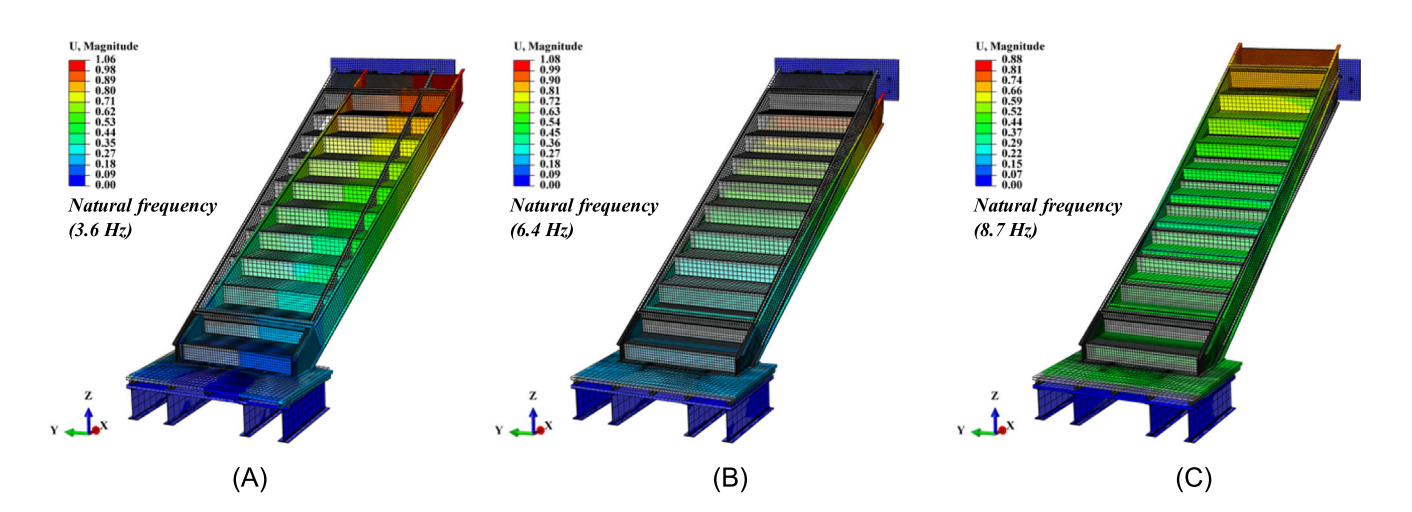


FIGURE 13 Mode shapes of the fixed-drift compatible stair system: (A) 1st mode, (B) 2nd mode, (C) 3rd mode.

# 4.1.3 | Fixed-drift compatible stair system

The first three mode shapes of the stair system fixed at the bottom and with drift-compatible connections installed at the top landing to stair flight, predicted by Abaqus, are shown in Figure 13. The first mode of this stair system, with a natural frequency of 3.6 Hz, is transverse movement at the top of the stair system which is accommodated in part by rotation of the bottom landing. The second mode of this stair system with natural frequencies of 6.4 Hz corresponds to the vibration of stairs in the vertical direction. A combination of the vertical and torsional modes of the fixed-drift compatible stair system is the third vibration mode with a natural frequency of 8.7 Hz.

The amplitude of the FRF of the measured accelerations for this configuration is plotted in Figure 14. It is observed that the FEM predicted the vibrational natural frequencies well. However, tracking the magnitudes of FRF, it is shown that unlike FEM-prediction in which the first mode was predominantly due to vibration of stair flight in transverse to the stair flight direction, the magnitude of FRF at the first mode is happening in Z-direction. Since this mode of the stairs is of very

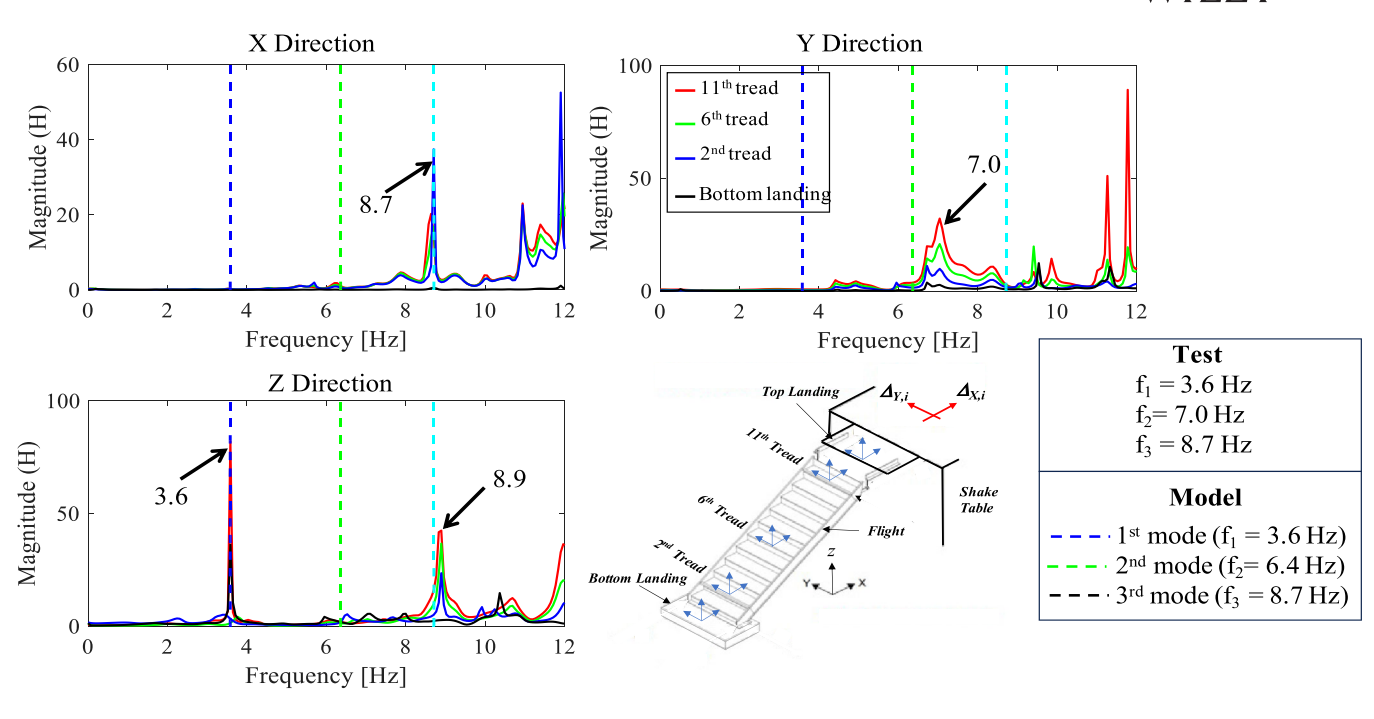


FIGURE 14 FRF computed using measured acceleration responses of fixed-drift compatible stair system. FRF, Frequency Response Function.

TABLE 4 Summary of natural frequencies of stair systems with various boundary conditions.

<b>Bottom connection</b>	Top connection	Mode	Test (Hz)	Model (Hz)	Description <sup>a</sup>
Fixed	Fixed	1	19	20.1	Transverse to flight (Y-direction, global)
Fixed	Fixed	2	39.5	36.5	Perpendicular to the stair flight (X and Z-directions, global)
Fixed	Fixed	3	N/A <sup>b</sup>	46.6	Torsional about flight (local)
Free	Fixed	1	13.9	14.5	Transverse to flight (Y-direction, global)
Free	Fixed	2	22.9	19.5	Transverse at bottom landing (local)
Free	Fixed	3	26.8	26.8	Perpendicular to the stair flight (X and Z-directions, global)
Fixed	Drift-compatible	1	3.6	3.6	Transverse to flight (Y-direction, global)
Fixed	Drift-compatible	2	7.0	6.4	Vertical along flight (Z-direction, global)
Fixed	Drift-compatible	3	8.7	8.7	Torsional + vertical along stair flight (local)

<sup>&</sup>lt;sup>a</sup>These mode descriptions are based on FEM prediction.

low frequency, it would have not been excited significantly. Relative to the fixed-fixed and the free-fixed stair systems, the fixed-drift compatible stair system is more flexible with smaller natural frequencies. For comparative purposes, a summary of the first three natural frequencies of each stair system with different boundary conditions is provided, see Table 4. It is worth mentioning that some of these estimated natural frequencies based on the peaks of the FRF plots are approximate as precise values may not be well defined, particularly for closely spaced modes.

# 4.2 | Dynamic response analyses

# 4.2.1 | Fixed-fixed stair system

The fixed-fixed stair system was tested under interstory drift histories as shown in Figure 15. In this test, the shake table input displacement was imposed only in the Y-direction. The displacements measured at the top and the bottom of the stair flight along with the FE analysis results are overlaid to facilitate comparison in Figure 16. It is worth noting, as

<sup>&</sup>lt;sup>b</sup>N/A = not available.

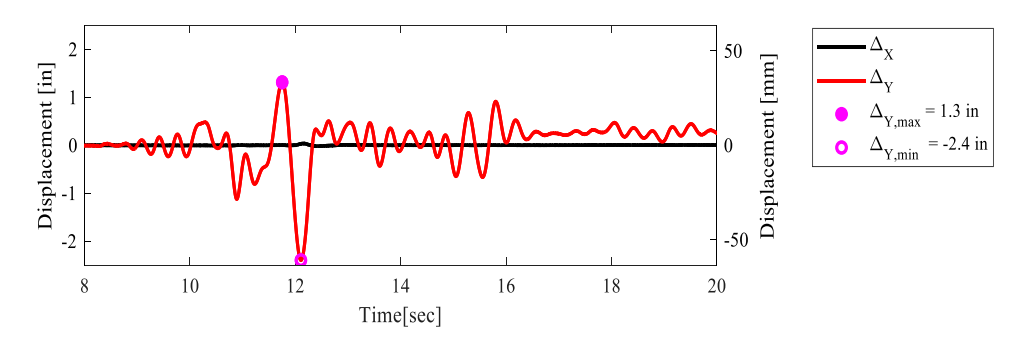


FIGURE 15 Input displacement time history for the fixed-fixed stair systems (1" = 25.4 mm).

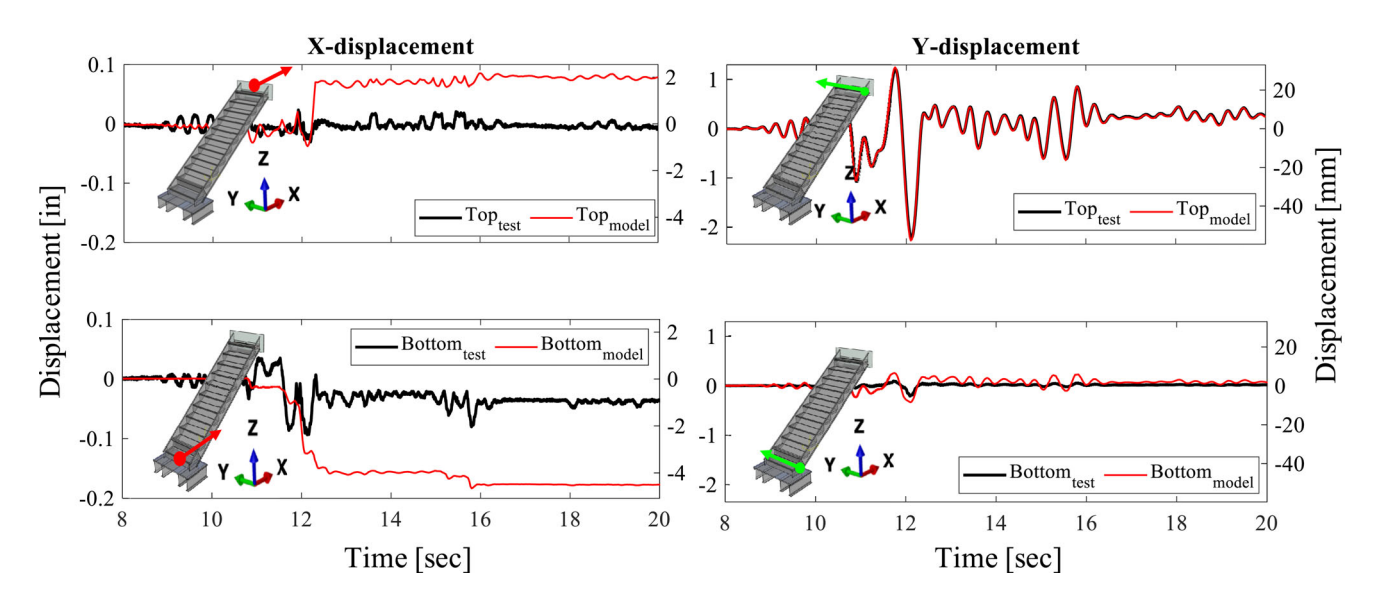


FIGURE 16 Measured displacement responses compared with FE analysis results for the fixed-fixed stair system. FE, finite element.

discussed in Section 2.3, that the displacement in X-direction at the top of the straight flight is the displacement of the stair flight relative to the top landing. However, all other displacements are absolute displacements. Observing both the test and analysis results, although the bottom connection was assumed to be fixed, the bottom of the stair flight moderately translated, in both X- and Y-directions, about 5% of the top landing movement. Considering the displacement at the top of the stair flight, in the Y-direction, the FEM predicted the experimental response with a high level of accuracy. This is consistent even under a large peak inter-story drift of 2.4 in (60.9 mm). Observing the relative displacement at the fixed ends, a larger difference between the FE and experimental results is observable. Nevertheless, comparing to the absolute displacements of the stair flight, the amplitudes of these relative displacements are much smaller (approximately 5% of the input interstory drift).

The acceleration responses of each stair system were recorded at five locations as discussed in Section 2.3. A fourth-order bandpass Butterworth filter with cut-off frequencies selected as 0.5 and 60 Hz was used to filter the measured acceleration responses. The measured peak accelerations overlaid with the FEM predictions at these five locations along the stair height are plotted in Figure 17. It is noted that, although the input displacement was purely in the Y-direction (transverse to the flight direction), the recorded peak accelerations on the stair flights in the X- and Z-directions are much higher than those in the Y-direction. Comparing the FE analysis results to the measured values, the analysis predicted the peak accelerations reasonably well. However, the FE analysis showed larger peak accelerations at the top landing. This is due to the large stiffness of the top-landing in the FEM as was discussed in Sections 3.1 and 3.2, adopted to simplify the top-landing, that is, modeled as a single plate with rigid material. Since, in this study, the dynamic analysis was displacement controlled, having a rigid top-landing would not affect the analysis result negatively.

FIGURE 17 Peak absolute acceleration profile for the fixed-fixed stair system.

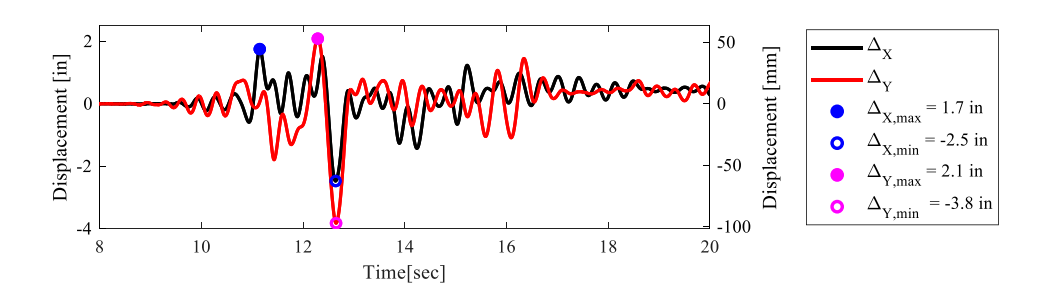


FIGURE 18 Input displacement time histories for the free-fixed stair system (Test 2) (1" = 25.4 mm).

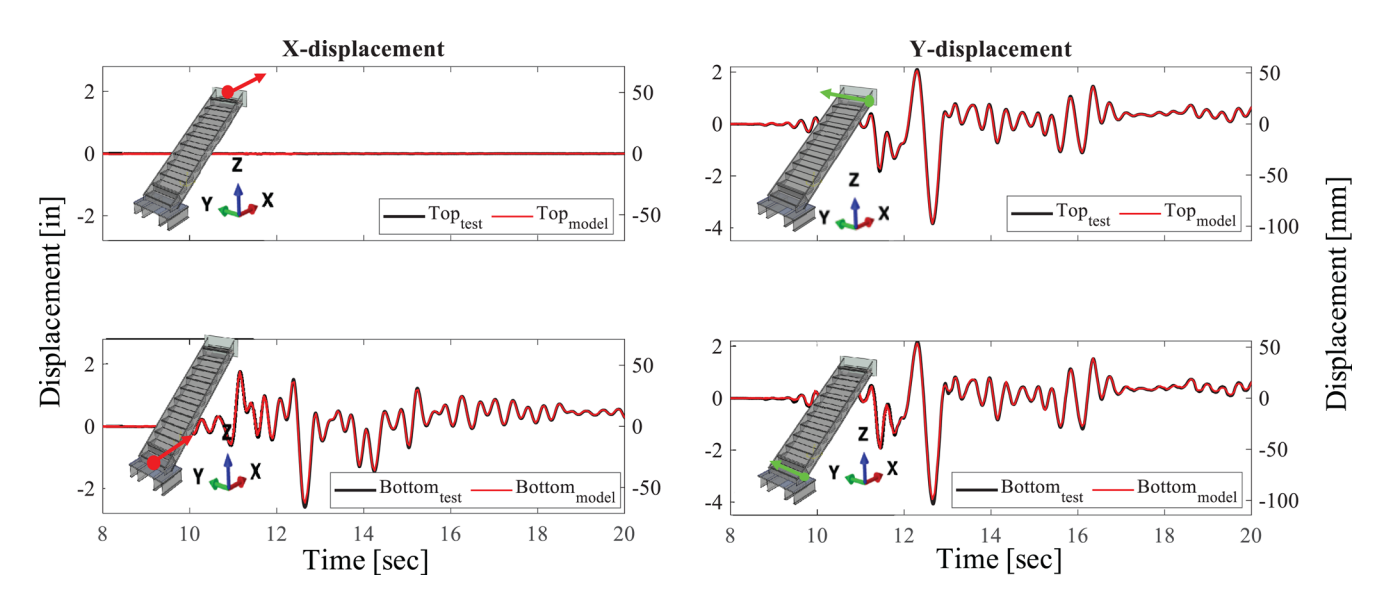


FIGURE 19 Measured displacement responses versus analysis results for the free-fixed stair system (Test 2).

# 4.2.2 | Free-fixed stair system

The free-fixed stair system was tested under three different bidirectional interstory drift histories (Table 1). Figure 18 shows the input displacement time histories of Test 2, while Figure 19 presents a comparison for this test of the displacement responses of the stair with the FE analysis results. The free movement of the stair flight on the bottom landing can be observed from the displacement time histories of the bottom of the stair flight in both the X- and Y-directions. Nevertheless, the transverse displacement of the stair flight at the bottom landing connection is slightly larger than that of the stair flight

FIGURE 20 Peak absolute acceleration profile for the free-fixed stair system (Test 2).

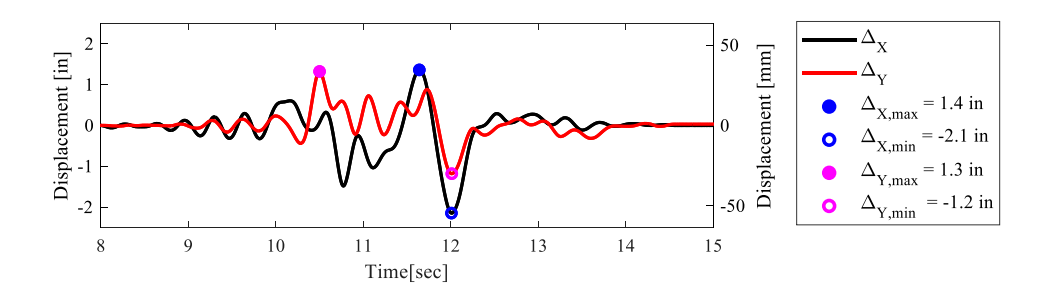


FIGURE 21 Input displacement time histories for the fixed-drift compatible stair system (Test 3) (1" = 25.4 mm).

near the top landing connection. This displacement amplification was higher during the tests under the combination of live and lateral loads. In addition, in the free-fixed stair system, unlike the fixed-fixed stair system, no movement of the stair flight relative to the top landing is observed. The FEM in this configuration predicted the deflection of the stair accurately even under a peak interstory drift of 3.8 in (97.2 mm).

The maximum accelerations recorded at five locations throughout the stair height are plotted in Figure 20. During Test 2, despite maximum interstory drifts of 3.8 in (97.2 mm), the peak accelerations in X- and Y-directions throughout the stair flight remain nearly constant. The free movement of the stair flight in both X- and Y-directions is the reason behind these constant acceleration profiles. Observing the peak accelerations recorded in the bottom landing, it is seen that the peak accelerations in the X- and Z-directions are approximately zero. This is due to the fact that the bottom landing is fixed in both X- and Z-directions, and no movement of the bottom landing in these directions is observed. However, at this location, the peak acceleration in the Y-direction is 0.35 g. Low stiffness of I-beams at the bottom landing, in the Y-direction, results in deflection and non-zero acceleration in the Y-direction. Observing the measured peak accelerations in Z-direction the acceleration is amplified, relative to top-landing, on the stair flight. The plot labeled as Model shows the FE analysis results in which the input interstory drift is the same as Test-2. The analysis predicted the peak accelerations reasonably well. However, like the FEM of the fixed-fixed stair system, the predicted peak accelerations, in the X- and Y-direction, at the top landing are larger than the measured ones. This is caused by the simplification of the top landing as discussed in Sections 3.1 and 3.2.

## 4.2.3 | Fixed-drift compatible stair system

To evaluate the performance of the FEM of the stair system with bottom connections fixed and drift-compatible connections installed in flight to top-landing connection, the responses of the stair under biaxial drift time histories (Test 3 in Table 2) were studied. Specifically, the input displacement time histories of Test 3 are shown in Figure 21, while the measured displacements at the top and the bottom of the stair flight, along with the analysis results, are shown in Figure 22. Observing the measured displacement time history at the top of the stair flight, in the Y-direction, a residual drift of 0.35 inches (8.9 mm) is visible. Since no yielding of the stair components was observed, this residual drift is either due to a slip in the stair flight to the bottom landing connection or displacement of the bottom landing plate relative to its sup-

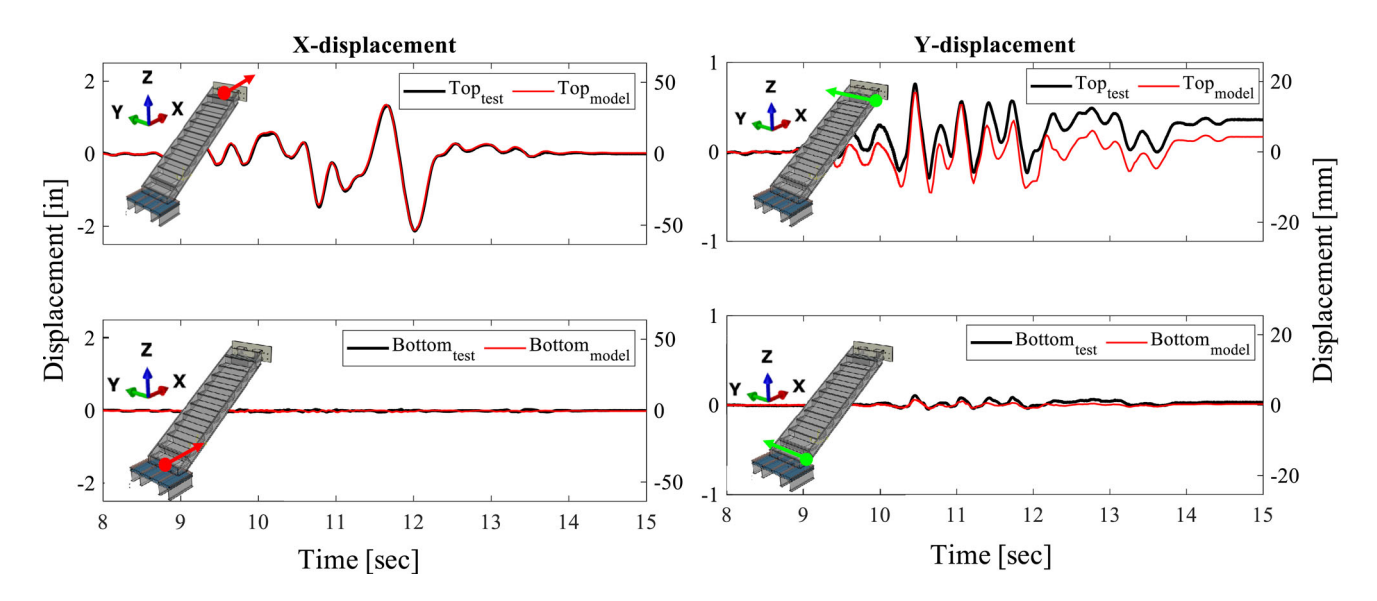


FIGURE 22 Measured displacement responses versus analysis results for the fixed-drift compatible stair system (Test 3).

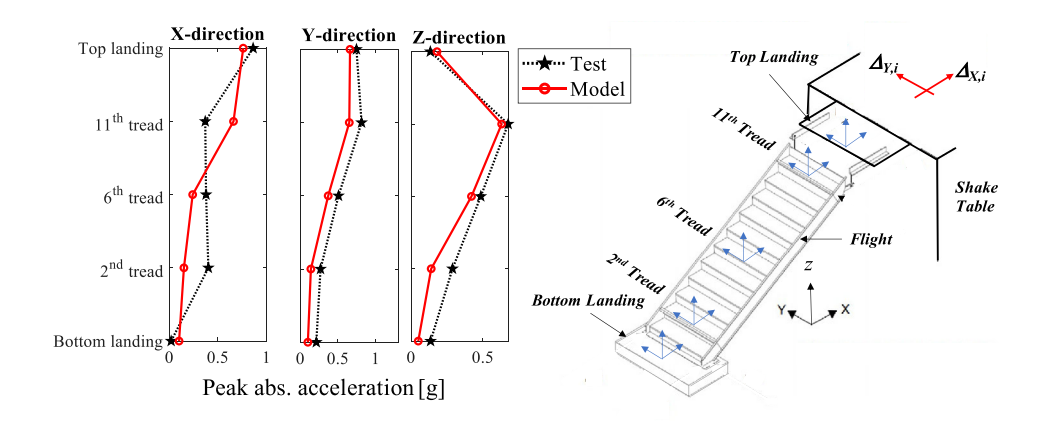


FIGURE 23 Peak absolute acceleration profile for the fixed-drift compatible stair system (Test 3).

porting HSS tubes. To allow a small rotation of the bottom landing, two springs in each of the X- and Y-directions were used in the FEM. To capture the observed response, bolt pre-tensioning load and spring stiffnesses were calibrated. The responses shown in Figure 22 are from the model with a spring stiffness of 5 kips/in (876 N/mm). In this analysis, the bolts were pre-tensioned with 65% of the yield strength of the bolt. Despite the nominal rotation of the stair flight during the experiments, the displacement of the stair flight in the Y-direction was captured with reasonable accuracy. In addition, the FEM predicted the displacement of the stair flight relative to the top landing, in the X-direction, with high level of accuracy. The displacement time histories at the top of the stair flight, in X-direction, facilitated the free movement of the top landing relative to the stair flight, and this feature resulted reasonable prediction of the overall stair system response for this connection configuration. However, observing the displacement time histories of the stair flight in the transverse direction (Y-direction), it is seen that approximately 50% of the top-landing movement is accommodated.

The peak accelerations along the stair height are shown in Figure 23. These results demonstrate that the accelerations in the X- and Y-directions are not amplified, relative to the top landing, along the stair flight, with the exception of small amplifications near the top landing, that is, at the 11th tread. Nonetheless, the peak acceleration amplifications are much smaller than that observed when the stair system is fixed at both ends. Observing the peak accelerations at the bottom landing in Y- and Z- directions, there is a non-zero peak acceleration which is likely due to the movements of the bottom landing plate in these directions. The plots labeled as Model show the analysis results in which the input interstory drift is the same as Test-3, which in this case articulates a very reasonable FEM prediction of the peak accelerations. There are small differences because these stair systems were tested many times and the FEM is based on the state of stairs without



being exposed to external loads. In addition, as is seen in Figure 23, the predicted peak accelerations at the top landing are not as large as was the case for the fixed-fixed and free-fixed stair systems because these accelerations were determined from a node on the attachment plate at the top landing.

#### 5 | CONCLUSIONS

Stair systems are the primary egress means during and following an earthquake. Unfortunately, prior earthquake events and experimental investigations continue to demonstrate that these essential nonstructural systems are prone to damage. Since stair systems span from floor to floor, they are exposed to multiple support dynamic excitation during an earthquake. To this end, the ASCE 7-16<sup>12</sup> standard requires stairs to be detailed to accommodate anticipated seismic relative displacement. In this regard, new connection concepts have been explored, with a particularly appealing approach involving releasing a stairs most significant boundary connections with the structural system. Experimental investigations between 2016-2018 explored such innovative connection "release" concepts. 14 Data from this shake table test program provide an opportunity to develop and evaluate the robustness of high-fidelity numerical models for use in future analytical investigations. Since the seismic response of stair systems strongly depends on the connection details such as the bolt's pre-tensioning forces, the friction responses between each element, the boundary conditions, and the material properties, it is essential to model the response of each element and the interaction between them accurately. In this regard, the present paper provides a brief overview of the two prior shake table test programs, <sup>14</sup> and the development of a suite of highfidelity FEMs for use in cross-comparison with these test results. The accuracy of the modeled fixed-fixed, free-fixed, and fixed-drift compatible stair systems was evaluated by comparing the analysis results with the measured responses. Based on the measured seismic responses of stairs and numerical simulation results, important observations are summarized as follows:

- Eigenvalue analysis results show that the first vibration mode of all straight-run stair systems studied corresponds to their vibration in the transverse to flight direction. The vibration mode in the vertical direction is subsequently consistently the second dominant mode; while torsional vibration modes are occurring at larger frequencies than the transverse and vertical vibration modes.
- The low stiffness of the bottom landing supports in the transverse to the stair flight direction contributes to the first mode of the fixed-fixed stair system, and the second mode of the free-fixed stair system. The natural frequencies of these two modes are approximately equal.
- In the case of fixed-fixed stair systems, although the input displacement time history was purely in the transverse to flight direction (Y-direction), considerably high accelerations, on the stair flight, in the parallel to flight (X-direction) and vertical (Z-direction) were observed.
- Observing the peak accelerations recorded on the bottom landing of the fixed-fixed and free-fixed stair systems, it is concluded that since the movement of the bottom landing in the X- and Z-directions was restrained, the accelerations in these directions are approximately zero. However, the supports of the bottom landing (I-beams) had a low stiffness in the Y-direction (transverse to flight direction). Therefore, movement of the bottom landing in this direction resulted in non-zero acceleration at the bottom landing. Both the eigenvalue and time history analyses indicate that the movement of the bottom landing in the Y-direction played an important role in the dynamic response of these stair systems.
- In the case of a free-fixed stair system, since the movement of the stair at the bottom connection is not constrained, the peak acceleration profiles along the stair height are approximately constant.
- In the stair system with a fixed bottom connection and a drift-compatible connection installed at the top landing to flight location, the drift-compatible connection allows free movement of the top landing in the longitudinal (X-direction). However, observing the response of the stair flight in the transverse direction (Y-direction), it is observed that approximately 50% of the top landing movement is accommodated. In addition, the amplification of accelerations, in both X-and Y-directions, on the stair flight is much smaller than that of the same stair assembly with a fixed-fixed connection configuration. This observed response, which is also captured with the high fidelity FEM, offers a beneficially seismic resilient stair system, which in the optimal case supports building seismic resiliency.

In summary, the proposed FEM was capable of capturing the dynamic characteristics of the stair systems with three types of flight-to-landing connections. Notably, the numerically predicted eigenvalues were in good agreement with

experimentally determined system identification results. In addition, the robustness of the FEM was demonstrated by performing nonlinear dynamic time history analysis and comparing results with measured responses obtained during shake table tests. It should be noted that careful considerations regarding the definition of elements, and material contacts are warranted in such FEM-based studies in particular to the sensitivity of the stair boundary conditions on response. The generally good agreement between model and experimental measurements utilizing the proposed modeling approach lends confidence towards development of larger FEMs of the stair system (e.g., multi-level stairs) or computationally efficient and reduced order FEMs that can be integrated into a building model to further investigate building-stair system interaction across different seismic hazard levels. For instance, Sorosh et al.<sup>19</sup> used the proposed FEM approach to predict the response of a scissor-type modular stair system with a drift-compatible connection, and two types of attachment strategies that were tested as part of the NHERI TallWood building in 2023 at the UC San Diego. In addition, the adaptation of the proposed FEM was presented in Sorosh et al.<sup>20</sup> to investigate the behavior of a new friction-based drift-compatible connection for stair systems.

#### **ACKNOWLEDGMENTS**

This study was supported by USFS Grant No. 19-DG-11046000-16. The first author received a graduate fellowship from the Department of Structural Engineering at the University of California San Diego. The authors appreciate this support. Opinions and findings of this study are of the authors and do not necessarily reflect those of the sponsors.

## DATA AVAILABILITY STATEMENT

Data may be provided if requested of authors.

#### ORCID

Shokrullah Sorosh https://orcid.org/0000-0003-2826-9696

Tara C. Hutchinson https://orcid.org/0000-0001-9109-7896

Keri L. Ryan https://orcid.org/0000-0002-0076-1630

#### REFERENCES

- 1. Li B, Mosalam KM. Seismic performance of reinforced concrete stairways during the 2008 Wenchuan earthquake. *ASCE J Perform Constr Facil*. 2013;27(6):721-730.
- 2. Beca Carter Hollings Ferner Ltd. Investigation into the collapse of the Forsyth Barr building stairs on 22nd February 2011. Tech. Rep. Technical Report BUI.COL764.0003A, A report at the Department of Building and Housing (DBH); 2011.
- 3. Bull D. Stair and access ramps between floors in multi-storey building. Tech. Rep. Technical Report ENG.BULL.0001, A report at the Canterbury Earthquake Royal Commission; 2011.
- 4. Higgins C. Prefabricated steel stair performance under combined seismic and gravity loads. ASCE J Struct Eng. 2009;135(2):122-129.
- 5. Hutchinson TC, Restrepo JI, Conte J, Meacham B. Overview of the building nonstructural component and systems (BNCS) project. In: Proc., ASCE 2013 Structures Congress. ASCE; 2013:1485-1498.
- 6. Wang X, Ebrahimian H, Astroza R, Conte J, Restrepo J, Hutchinson TC. Shake table testing of a full-scale five-story building: pre-test simulation of the test building and development of a nonstructural component and systems design criteria. In: Proc., ASCE Structures Congress. ASCE; 2013.
- 7. Wang X, Astroza R, Hutchinson TC, Conte JP, Restrepo JI. Dynamic characteristics and seismic behavior of prefabricated steel stairs in a full-scale five-story building shake table test program. *Earthquake Eng Struct Dyn.* 2015;44(14):2507-2527.
- 8. Sun H, Zhang A, Cao J. Earthquake response analysis for stairs about frame structure. Eng Fail Anal. 2013;33(2013):490-496.
- 9. Tegos IA, Panoskaltsis VP, Tegou SD. Analysis and design of staircases against seismic loadings. In: Proc., 4th ECCOMAS thematic conference on computational methods in structural dynamics and earthquake engineering. Eccomas Proceedia; 2013.
- 10. Noorifard A, Tabeshpour MR. Effects of staircase on the seismic behavior of RC moment frame buildings. *Archit Civil Eng Environ*. 2018;11(2018)(4):105-122.
- 11. Wang X, Hutchinson TC. Computational assessment of the seismic behavior of steel stairs. Eng Struct. 2018;166(2018):376-386.
- 12. ASCE 7-16. Minimum Design Loads and Associated Criteria for Buildings and Other Structures. Standard ASCE/SEI 7-16, Structural Engineering Institute of American Society of Civil Engineers; 2017.
- 13. Black C, Aiken I, Smith K, Belvin R, Peachey A. Seismically-Resilient Stair Systems for Buildings. In: Proc., Structural Engineers Association of California Annual Convention. SEAOC; 2017.
- 14. Black C, Aiken I, Smith K, Belvin R, Peachey A. Shake table testing of seismically resilient stair systems for buildings. In: Proc., 17th World Conference on Earthquake Engineering. 2020.
- 15. Construction Specialties Inc. Shake-Table Testing of Construction Specialties DriftReady<sup>TM</sup> Stair Systems. CS-Group; 2018. Accessed January 2021. www.c-sgroup.com
- 16. Abaqus. Abaqus Documentation, Software Manual. Dassault Systems; 2020.

- 17. Barrett RT. Fastener Design Manual. Tech. Rep. NASA Reference Publication 1228; 1990.
- 18. Sun EQ. Shear Locking and Hourglassing in MSC, Nastran, ABAQUS. MSC Software Users Meeting; 2006.
- 19. Sorosh S, Hutchinson TC, Ryan KL, et al. Numerical Simulation of Prefabricated Steel Stairs to be Implemented in the NHERI TallWood Building. In: Fifth International Workshop on the Seismic Performance of Non-StructuralElements (SPONSE). SPONSE; 2022.
- 20. Sorosh S, Hutchinson TC, Smith K, Kovac A. Advancing resilient stair systems considering friction-based drift-compatible connections. In: 18th World Conference on Earthquake Engineering. 2024.

**How to cite this article:** Sorosh S, Hutchinson TC, Ryan KL, Smith K, Belvin R, Black C. High-fidelity finite element modeling of the seismic response of prefabricated steel stairs. *Earthquake Engng Struct Dyn*. 2024;53:2491–2510. https://doi.org/10.1002/eqe.4117